

© 2018 American Meteorological Society. For information regarding reuse of this content and general copyright information, consult the [AMS Copyright Policy](https://www.ametsoc.org/PUBSReuseLicenses) ([www.ametsoc.org/PUBSReuseLicenses](https://www.ametsoc.org/PUBSReuseLicenses)).

# A Functional Response Metric for the Temperature Sensitivity of Tropical Ecosystems

**Gretchen Keppel-Aleks<sup>a</sup> and Samantha J. Basile**

Climate and Space Sciences and Engineering, University of Michigan, Ann Arbor, Michigan

**Forrest M. Hoffman**

Computational Earth Sciences Group, and Climate Change Science Institute, Oak Ridge National Laboratory, Oak Ridge, and Department of Civil & Environmental Engineering, University of Tennessee, Knoxville, Tennessee

Received 11 July 2017; in final form 10 February 2018

**ABSTRACT:** Earth system models (ESMs) simulate a large spread in carbon cycle feedbacks to climate change, particularly in their prediction of cumulative changes in terrestrial carbon storage. Evaluating the performance of ESMs against observations and assessing the likelihood of long-term climate predictions are crucial for model development. Here, we assessed the use of atmospheric CO<sub>2</sub> growth rate variations to evaluate the sensitivity of tropical ecosystem carbon fluxes to interannual temperature variations. We found that the temperature sensitivity of the observed CO<sub>2</sub> growth rate depended on the time scales over which atmospheric CO<sub>2</sub> observations were averaged. The temperature sensitivity of the CO<sub>2</sub> growth rate during Northern Hemisphere winter is most directly related to the tropical carbon flux sensitivity since winter

---

<sup>a</sup>Corresponding author: Gretchen Keppel-Aleks, [gkeppela@umich.edu](mailto:gkeppela@umich.edu)

variations in Northern Hemisphere carbon fluxes are relatively small. This metric can be used to test the fidelity of interactions between the physical climate system and terrestrial ecosystems within ESMs, which is especially important since the short-term relationship between ecosystem fluxes and temperature stress may be related to the long-term feedbacks between ecosystems and climate. If the interannual temperature sensitivity is used to constrain long-term temperature responses, the inferred sensitivity may be biased by 20%, unless the seasonality of the relationship between the observed CO<sub>2</sub> growth rate and tropical fluxes is taken into account. These results suggest that atmospheric data can be used directly to evaluate regional land fluxes from ESMs, but underscore that the interaction between the time scales for land surface processes and those for atmospheric processes must be considered.

**KEYWORDS:** Tropics; Carbon dioxide; Climate models; Model evaluation/performance; Atmosphere-land interaction; Ecosystem effects

## 1. Introduction

Evaluating feedbacks between tropical ecosystems and long-term climate change is crucial since terrestrial ecosystems currently act as a sink for 25%–30% of annual fossil fuel emissions (Le Quéré et al. 2016), and humid and semiarid tropical ecosystems are thought to contribute substantially to both the mean strength and the interannual variability of the sink (Ahlström et al. 2015). Several studies have noted that these ecosystems are highly sensitive to variations in temperature (Cox et al. 2013; Wang et al. 2013) and drought stress (Phillips et al. 2009; Gatti et al. 2014), suggesting that the tropical sink may be modified by changing climate. Tropical ecosystems store an estimated 500 PgC as biomass that may be vulnerable to long-term climate change (Pan et al. 2011), since under a high temperature future, ecosystem carbon loss due to higher tree mortality or enhanced rates of heterotrophic respiration may exceed net uptake by plants. Moreover, gross ecosystem fluxes in the tropics are large, between 50% and 60% of global primary productivity (Beer et al. 2010), suggesting that even small changes in climate could have a large impact on global carbon uptake. Recent studies have suggested that improving observational inferences about tropical carbon–climate interactions is necessary, since these ecosystems may be near a high temperature threshold in which further increases to air temperature reduce net assimilation (Doughty and Goulden 2008).

Long-term changes in land carbon stocks ( $\Delta C_L$ ; equivalent to cumulative net fluxes) are commonly attributed to a carbon–concentration feedback and a carbon–climate feedback [Boer and Arora (2009); Equation (1)]:

$$\Delta C_L = \beta \Delta \text{CO}_2 + \gamma_{LT} \Delta T, \quad (1)$$

where  $\beta$  [PgC ppm<sup>-1</sup>] represents the sensitivity of land carbon stocks to CO<sub>2</sub> fertilization, and  $\gamma_{LT}$  [PgC K<sup>-1</sup>] represents their sensitivity to long-term temperature changes  $\Delta T$  (Friedlingstein et al. 2006). Coupled Earth system model (ESM) predictions of  $\Delta C_L$  through 2100 vary widely and do not even agree in sign (Friedlingstein et al. 2006, 2014). The mechanistic attribution for  $\Delta C_L$  among ESMs participating in phase 5 of the Coupled Model Intercomparison Project (CMIP5; Taylor et al. 2012) likewise disagreed: model  $\beta$  factors differed by a

factor of 6, while model  $\gamma_{LT}$  coefficients differed by a factor of 5 (Arora et al. 2013).

The lack of model agreement in both the magnitude of and the mechanism driving the land carbon feedback to anthropogenic climate change underscores the need to evaluate models against observations. When evaluating coupled ESMs, simulated ecosystem properties may disagree with observational metrics due either to misparameterization of the relevant biogeochemical or biogeophysical processes or to biases in the physical climate drivers thereof. Model development and improvement, therefore, requires evaluating simulations using metrics that constrain functional responses—in other words, the relationships between driver and response variables—rather than simply comparing time series or spatial distributions of individual variables (Randerson et al. 2009).

It is further necessary to identify methods to gauge the realism of future predictions, since model agreement with present-day observations merely improves confidence that the model represents relevant processes, but cannot ensure predictive skill (Tebaldi and Knutti 2007; Bonan and Doney 2018). One method that has become increasingly prominent in climate change literature is the use of emergent constraints, which provides a methodology to evaluate long-term predictions within the context of a multimodel ensemble when a correlation exists between a short-term functional response, which can be evaluated against observations, and a long-term feedback governed by the same mechanism (Klein and Hall 2015). For example, Hoffman et al. (2014) showed that in the CMIP5 ensemble of ESMs, the atmospheric CO<sub>2</sub> mole fraction at 2100 was correlated to the simulated mole fraction in 2010. This relationship forms the basis for an emergent constraint because 1) the accuracy of the short-term model output (CO<sub>2</sub> at 2010) can be evaluated against observations, and 2) the same processes that govern the rate of atmospheric carbon accumulation through 2010 [viz., the magnitude of the  $\beta$  and  $\gamma_{LT}$  effects in Equation (1)] are among the important processes that govern atmospheric carbon accumulation through 2100. While this example relates to carbon cycle feedbacks, emergent constraints have been used to evaluate the likelihood of long-term predictions for several different components of the Earth system, including cryospheric feedbacks (Hall and Qu 2006; Boé et al. 2009) and cloud feedbacks (Gordon and Klein 2014) to climate change.

Unfortunately, developing functional response metrics for tropical ecosystem carbon–climate interactions is difficult, in part because of a lack of large-scale observations of tropical ecosystem function. There are limited tropical sites at which fluxes are measured directly via eddy covariance (Schimel et al. 2015). Moreover, these sites may not be representative of the entire tropics, given a high degree of ecosystem heterogeneity driven both by biological diversity and abiotic factors, such as soil chemistry and local hydrology (e.g., Araujo et al. 2002; Townsend et al. 2008). Thus, we propose to exploit long-term observations of the atmospheric CO<sub>2</sub> mole fraction to gain insight into functional relationships within tropical ecosystems. The atmospheric CO<sub>2</sub> mole fraction, which can be observed in situ, measured via flask sampling, or inferred from remote sensing, integrates variations in fluxes at spatial scales compatible with the resolution of ESMs (on the order of 10<sup>4</sup> to 10<sup>6</sup> km<sup>2</sup>) (Keppel-Aleks et al. 2013). Given the large concentration footprint, atmospheric CO<sub>2</sub> variations in space and time are an apt constraint for regional- to global-scale carbon–climate feedbacks (Keppel-Aleks et al. 2013). A

**Table 1. Metrics for carbon–climate feedbacks**

	Symbol	Units	Application
Long-term carbon cycle feedbacks	$\gamma_{LT}$	PgC K <sup>-1</sup>	Temperature sensitivity of land carbon stocks to long-term climate change
	$\beta$	PgC ppm <sup>-1</sup>	Fertilization effect of enhanced atmospheric CO <sub>2</sub> on land carbon stocks
Functional response diagnostics	$\gamma_{IAV}^{obs}$	PgC yr <sup>-1</sup> K <sup>-1</sup>	Interannual sensitivity from observations; must be inferred from atmospheric data
	$\gamma_{IAV}$	PgC yr <sup>-1</sup> K <sup>-1</sup>	Interannual sensitivity from simulations; can be inferred either from integrated fluxes or from simulated atmospheric CO <sub>2</sub>
Emergent constraint diagnostic	$\gamma_{LT}^{opt}$	PgC K <sup>-1</sup>	Temperature sensitivity of land carbon stocks to long-term climate change constrained by model agreement with $\gamma_{IAV}^{obs}$

previous study that analyzed variations in atmospheric CO<sub>2</sub>, its isotopic composition, and the atmospheric O<sub>2</sub> mole fraction at both seasonal and interannual time scales found terrestrial, rather than oceanic, fluxes are the primary drivers of variations in the atmospheric CO<sub>2</sub> mole fraction (Battle et al. 2000), a result corroborated by atmospheric inverse modeling of both CO<sub>2</sub> and its isotopic composition (Rayner et al. 2008). At interannual time scales, therefore, variability in the atmospheric CO<sub>2</sub> growth rate may be used to estimate the sensitivity of terrestrial ecosystems to variations in climate (Wang et al. 2013; Keppel-Aleks et al. 2014).

Several studies have shown that the single variable to which the interannual CO<sub>2</sub> growth rate is most strongly correlated is tropical temperature variations, suggesting high temperature stress in tropical ecosystems (Wang et al. 2013). Cox et al. (2013) further showed a strong correlation between interannual growth rate sensitivity to temperature ( $\gamma_{IAV}$ ; Table 1) and long-term carbon losses in response to warming  $\gamma_{LT}$  [Table 1; Equation (1)] across C<sup>4</sup>MIP coupled models. By using 50 years of atmospheric CO<sub>2</sub> observations to identify the models whose  $\gamma_{IAV}$  was consistent with the observationally derived temperature sensitivity, Cox et al. (2013) concluded that the most likely long-term sensitivity to warming was weaker than that of the unconstrained multimodel mean and had narrower uncertainty. More recently, Wenzel et al. (2014) applied the same method to the CMIP5 ensemble and found that the constrained value on  $\gamma_{LT}$  was consistent between the two model ensembles.

While the use of emergent constraints provides a promising method to link contemporary observations to the likelihood of future model outcomes, the results must be interpreted with caution. Previous studies have acknowledged that different processes, including vegetation mortality and shifts in vegetation, operate at long time scales, which could cause decoupling between the short-term and long-term temperature responses (Randerson 2013). Here, we focus on the challenge of evaluating modeled land fluxes against observed atmospheric CO<sub>2</sub> since atmospheric CO<sub>2</sub> reflects additional processes, such as atmospheric mixing, that are characterized by time scales independent of those that affect terrestrial ecosystems. Furthermore, atmospheric CO<sub>2</sub> contains the imprint of drought, temperature, and fire across the tropics and the Northern Hemisphere (NH) (Keppel-Aleks et al. 2014; Wunch et al. 2013), so accounting for the influence of these drivers on

atmospheric growth rate variability is necessary in developing a functional response metric focused on tropical ecosystems.

The goal of this paper is to identify methods to use atmospheric CO<sub>2</sub> observations to isolate the temperature sensitivity of tropical net terrestrial exchange ( $\gamma_{\text{IAV}}^{\text{obs}}$ ; defined in Table 1). As a second step, we seek to quantify the difference between using land fluxes and atmospheric CO<sub>2</sub> observations for calculating the  $\gamma_{\text{IAV}}$  from simulations. Finally, we extend the application of this metric as an emergent constraint for the long-term temperature sensitivity ( $\gamma_{\text{LT}}$ ; Table 1); this step will permit quantification of the uncertainty embedded in the emergent constraint approach due to uncertainties in the observational constraint. Overall, we hypothesize that any dissimilarity between the model output used to quantify short-term variations and the observations used as benchmarks may contribute bias both to the functional response metric and to the emergent constraint. For example, Cox et al. (2013) spatially integrated global land fluxes to represent the variation in atmospheric CO<sub>2</sub>, implicitly assuming the atmosphere is instantaneously well mixed. In reality, atmospheric CO<sub>2</sub> varies with location due to atmospheric transport patterns and is sampled only at discrete points in space and time. The  $\gamma_{\text{IAV}}$  estimated from atmospheric CO<sub>2</sub> therefore depends on the extent of spatial and temporal averaging of the observations (Keppel-Aleks et al. 2014). The structure of the paper is as follows: in section 2, we describe the method to calculate CO<sub>2</sub> interannual variability and its relationship to temperature for both observations and ESMs. In section 3, we report results using atmospheric observations for benchmarking ESM sensitivities. Finally, in section 4, we describe implications for using atmospheric CO<sub>2</sub> as a benchmark for functional responses and requirements for future model development.

## 2. Methods

### 2.1. CO<sub>2</sub> growth rate from atmospheric observations

We calculated the temperature sensitivity of the atmospheric CO<sub>2</sub> mole fraction growth rate derived from observations at marine boundary layer (MBL) sites in the NOAA network (Dlugokencky et al. 2016; Table 2). These sites are located away from fossil fuel sources and regions of strong terrestrial uptake, and monthly mean data are derived from flask samples that are accurate to within 0.2 ppm of the WMO scale with a  $1\sigma$  precision of 0.1 ppm (Conway et al. 1994). We calculated the interannual component of variability by detrending the monthly mean CO<sub>2</sub> time series from each site, using a 3rd-order polynomial over the 24-yr period from 1982 to 2005 and then subtracting the mean annual cycle (Keppel-Aleks et al. 2013). Site-specific interannual variability [IAV (ppm)] was averaged within six latitude belts corresponding to the tropics (0°–23°), midlatitudes (23°–60°), and high latitudes (60°–90°) of each hemisphere, and a global mean time series of CO<sub>2</sub> variability was then calculated as the area-weighted average of IAV within these latitude belts (Figure 1). We analyzed the time period after 1982 since there are multiple observing sites within all latitude belts. Furthermore, our zonal averaging approach ensured that the globally averaged CO<sub>2</sub> variability was not overly influenced by the Northern Hemisphere, where the sampling network is more dense. For consistency with previous work (e.g., Cox et al. 2013; Wang et al. 2013; Wenzel et al.

**Table 2. NOAA flask sampling sites within the MBL used in this analysis. Sites were selected with nearly continuous data coverage between 1982 and 2005, the end of the historical period for CMIP5 models.**

Region	Station	Acronym	Lat	Lon
60°–90°N	Alert, AK	ALT	82.5	–62.5
	Ny-Ålesund, Svalbard	ZEP	78.9	11.9
	Barrow, AK	BRW	71.3	–156.6
	Stórhöfði, Iceland	ICE	63.4	–20.1
23°–60°N	Mace Head, Ireland	MHD	53.3	–9.9
	Shemya, AK	SHM	52.7	174.1
	Terceira Island, Azores	AZR	38.8	–27.4
	Tudor Hill, Bermuda	BMW	32.3	–64.7
	Sand Island, Midway	MID	28.2	–177.4
	Key Biscayne, FL	KEY	25.7	–80.2
	Pacific Ocean 25°N	POCN25	20.0	221.0
	0°–23°N	Pacific Ocean 20°N	POCN20	20.0
Cape Kumukahi, HI		KUM	19.5	–155.6
Pacific Ocean 15°N		POCN15	15.0	217.0
Mariana Islands, Guam		GMI	13.4	144.8
Ragged Point, Barbados		RPB	13.2	–59.4
Pacific Ocean 10°N		POCN10	10.0	213.0
Pacific Ocean 5°N		POCN05	5.0	209.0
Christmas Island		CHR	1.7	202.8
0°–23°S	Seychelles	SEY	–4.7	55.2
	Pacific Ocean 5°S	POCS05	–5.0	201.0
	Ascension Island	ASC	–8.0	–14.4
	Pacific Ocean 10°S	POCS10	–10.0	197.0
	Tutuila, American Samoa	SMO	–14.3	–170.6
	Pacific Ocean 15°S	POCS15	–15.0	193.0
23°–60°S	Pacific Ocean 20°S	POCS20	–20.0	189.0
	Pacific Ocean 25°S	POCS25	–25.0	186.0
	Pacific Ocean 30°S	POCS30	–30.0	183.0
	Pacific Ocean 35°S	POCS35	–35.0	–180.0
	Cape Grim, Australia	CGO	–40.7	144.7
	Baring Head	BHD	–41	174
	Crozet Island	CRZ	–46.45	51.85
60°–90°S	Palmer Station, Antarctica	PSA	–64.0	–64.0
	Syowa, Antarctica	SYO	–69.0	39.6
	Halley Bay, Antarctica	HBA	–75.6	–26.5
	South Pole	SPO	–90.0	–24.8

2014), we filtered out CO<sub>2</sub> IAV from measurements during the 24 months following the major volcanic eruptions of El Chichon (1982) and Mt. Pinatubo (1991).

We aggregated the monthly mean CO<sub>2</sub> interannual variability into either quarters (e.g., January–March and April–June) or years and differenced across sequential periods to calculate a growth rate (ppm yr<sup>–1</sup>). The seasonal growth rate anomalies were therefore centered on 1 January (winter; difference between JFM and OND), 1 April (spring; difference between AMJ and JFM), 1 July (summer; difference between JAS and AMJ), and 1 October (fall; difference between OND and JAS), and the annual mean growth rate was centered on 1 January. Growth rate anomalies

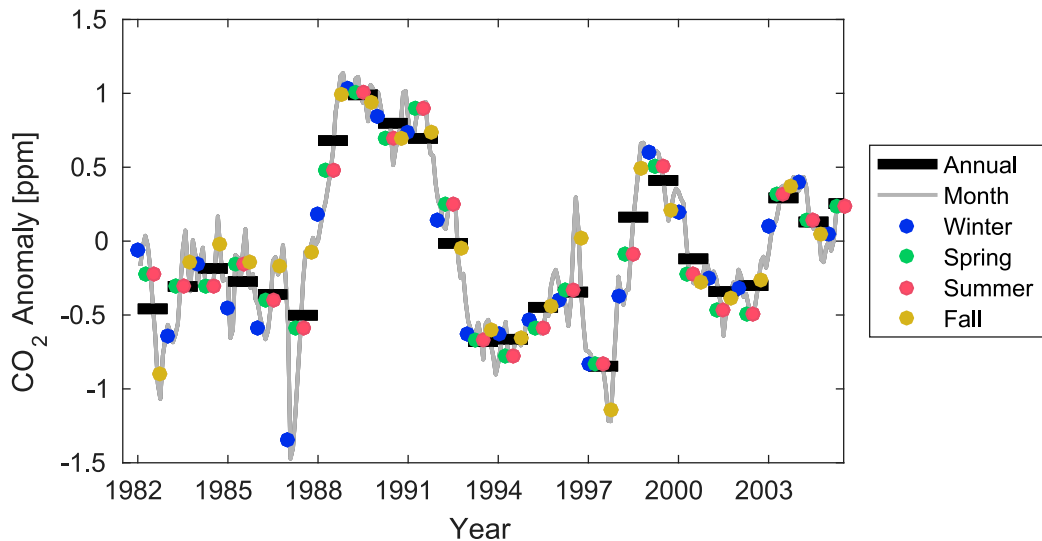


**Figure 1.** Time series of global atmospheric CO<sub>2</sub> interannual variability calculated at annual, quarterly, and monthly frequencies from MBL observatories.

at all temporal frequencies were then converted to units of PgC yr<sup>-1</sup> using the global mass of atmospheric dry air.

The interannual growth rate anomaly was related to variations in tropical temperature via linear regression to estimate  $\gamma_{IAV}$  (Figure 2). We calculated an area-weighted tropical land temperature between 23°S and 23°N using the gridded Hadley Centre Climate Research Unit (CRU) dataset at 4° × 5° resolution (Jones et al. 2012). The tropical land temperature time series was linearly detrended and the mean annual cycle removed to reveal interannual variations at monthly time steps, which were averaged to the same quarterly or annual resolution as the atmospheric CO<sub>2</sub> observations. Because the atmospheric CO<sub>2</sub> growth rate is calculated as a difference and therefore centered at the start of each quarter (e.g., 1 January and 1 April) or calendar year, and the temperature anomaly is centered midquarter or midyear, we averaged two successive quarters or years of temperature anomalies over land (cf. Cox et al. 2013) before calculating  $\gamma_{IAV}$  via linear regression of the two quantities.

Climate variability is not normally distributed, so the length of and gaps in the CO<sub>2</sub> and temperature records may affect the estimate of  $\gamma_{IAV}$ . We quantified uncertainty in the regression coefficient due to data gaps and outliers using bootstrap Monte Carlo to generate 1000 synthetic datasets of length 24 years by sampling observed CO<sub>2</sub>–temperature pairs with replacement, and we report the median and standard deviation of  $\gamma_{IAV}$  across these realizations. The same method was used to calculate  $\gamma_{IAV}$  from simulated carbon cycle diagnostics (section 2.2).

## 2.2. CMIP5 carbon cycle diagnostics

We analyzed the interannual climate sensitivity of terrestrial carbon uptake for historical simulations in eight CMIP5 ESMs (Table 3) whose outputs were

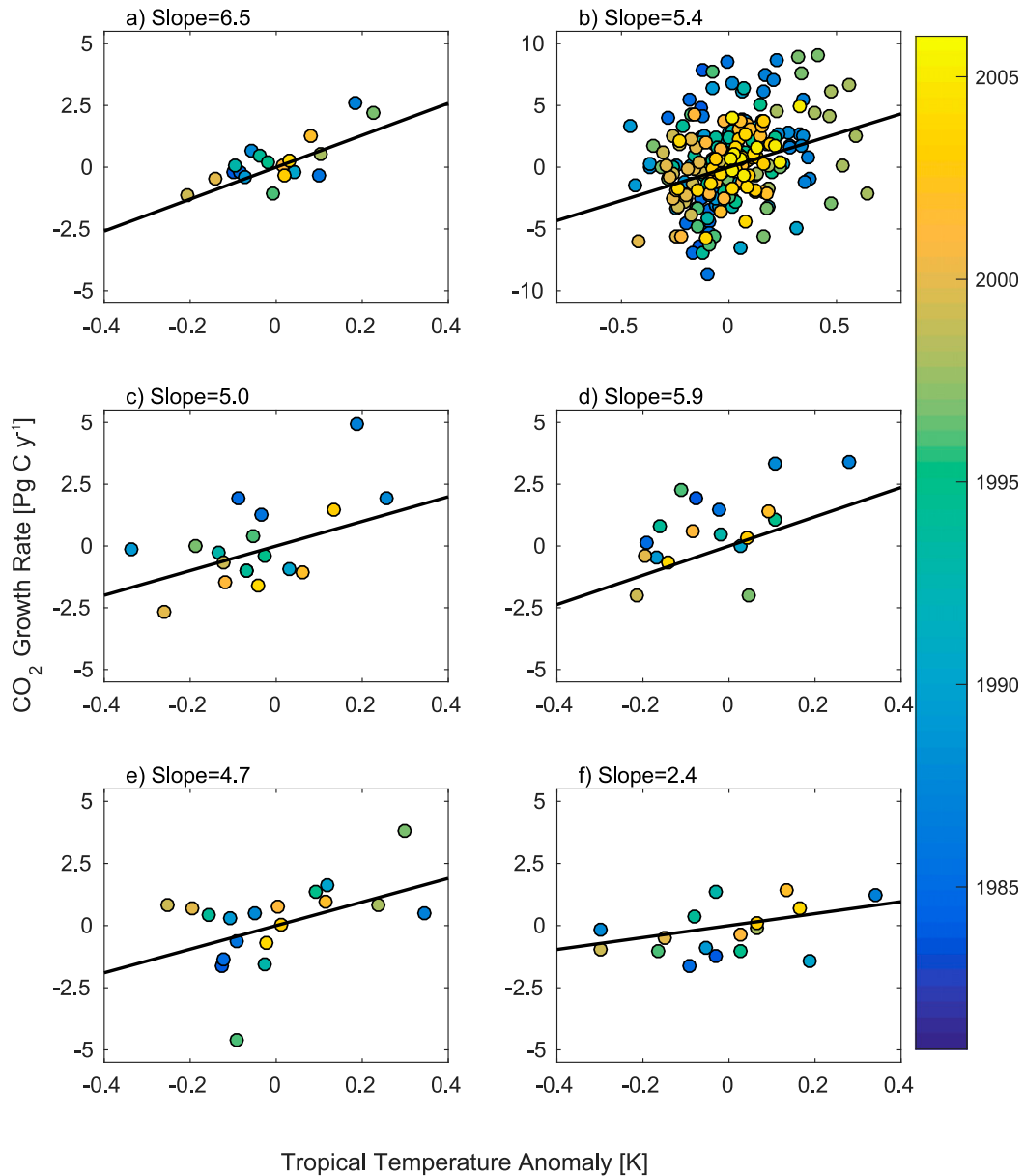


**Figure 2.** Relationship between the observed CO<sub>2</sub> growth rate anomaly and tropical temperature variations at (a) annual, (b) monthly, and seasonal time scales for (c) winter (JFM), (d) spring (AMJ), (e) summer (JAS), and (f) fall (OND). The  $\gamma_{IAV}$  value is given by the slope of the relationship in units PgC yr<sup>-1</sup> K<sup>-1</sup>.

obtained from the Earth System Grid Federation (Williams et al. 2011). The historical simulations covered the period 1850–2005 and were forced with historical atmospheric composition changes, including greenhouse gas and aerosol concentrations resulting from anthropogenic and natural sources. CMIP5 models were

**Table 3. CMIP5 models and the temperature sensitivities of land carbon processes. CMIP5 temperature sensitivities have been calculated directly from simulated land fluxes and indirectly using simulated atmospheric CO<sub>2</sub>. The observed temperature sensitivities are calculated only from atmospheric CO<sub>2</sub>.**

Model name	$\gamma_{LT}$ [PgC K <sup>-1</sup> ]	$\gamma_{IAV}$ [PgC yr <sup>-1</sup> K <sup>-1</sup> ]			
		Global NBP	Tropical NBP	Annual CO <sub>2</sub>	Winter CO <sub>2</sub>
CESM	-6.7	0.9±1.1	0.9±0.8	1.9±1.4	1.9±0.8
CanESM2	-74.3	8.2±0.9	6.5±0.7	10.8±1.5	8.4±0.8
GFDL-ESM2G	-116.4	12.4±2.1	10.2±1.3	16.8±2.9	9.6±2.7
HadGEM2-ES	-60.2	8.2±1.2	8.1±1.3	7.5±1.6	7.1±1.4
IPSL-LR	-22.9	5.6±1.0	5.8±0.9	7.0±1.5	7.4±1.9
MIROC-ESM	-58.4	4.9±1.0	3.2±0.9	7.6±1.5	3.7±1.1
MPI	-78.3	5.4±0.6	2.8±0.3	6.7±0.6	2.1±0.6
NorESM	-7.2	3.2±1.6	3.1±1.1	4.2±2.3	2.9±1.3
Model mean	-53±38	6.1±3.5	7.8±4.6	7.0±3.8	7.2±3.4
Observations				6.5 ± 1.8	5.0 ± 2.0

also forced with historical land-use change patterns, although the implementation varied across models (Taylor et al. 2012). From these simulations, we analyzed temperature and net biospheric production (NBP) output. NBP encompasses all terrestrial processes that leave an imprint on atmospheric CO<sub>2</sub>, including net ecosystem exchange (NEE; defined as the sum of gross primary production and ecosystem respiration), carbon loss from disturbance, and harvest (Chapin et al. 2006). Each CMIP5 ESM is fully prognostic, meaning the carbon cycle in each model was coupled to different patterns of internal climate variability. Thus, evaluation of the interannual variability requires a functional response metric, since the timing and magnitude of internal climate variations, such as those from El Niño, are unique to each model run.

To examine our hypothesis that neglecting atmospheric processes induces a bias between  $\gamma_{IAV}$  inferred from modeled fluxes and the  $\gamma_{IAV}^{obs}$  that must be calculated from atmospheric CO<sub>2</sub>, it was necessary to use an offline atmospheric transport model to simulate atmospheric CO<sub>2</sub> at the MBL observatories since only a few CMIP5 models propagated surface carbon fluxes through their own atmospheric model. To simulate the imprint of transport, we used the GEOS-Chem atmospheric transport model (version 9.1.2; Nassar et al. 2010) to simulate the spatial distribution of CO<sub>2</sub> from CMIP5 NBP. GEOS-Chem was driven by MERRA reanalysis data (Rienecker et al. 2011) at 4°lat × 5°lon horizontal resolution, with NBP data from each CMIP5 model regridded to the resolution of the transport model. We ran the model from 1979 through 2005, discarding the first 3 years to allow for the CO<sub>2</sub> tracer to spin up. We then sampled monthly mean CO<sub>2</sub> output from GEOS-Chem at the locations of NOAA MBL sites and detrended the model output using the method described for the observations. Simulated  $\gamma_{IAV}$  values were likewise determined by regressing the CO<sub>2</sub> growth rate against each model’s tropical land temperature anomaly.

We note that in comparing the simulated atmospheric CO<sub>2</sub> to the observations, we neglect nonterrestrial influences on the observations. For example, the observed CO<sub>2</sub> growth rate anomaly includes a small contribution from ocean and fossil fluxes (Keppel-Aleks et al. 2014), while the simulated CO<sub>2</sub> growth rate includes only the influence of NBP. Thus, any covariance between temperature and ocean

carbon fluxes or fossil fuel emissions will modify  $\gamma_{IAV}^{obs}$  but none of the model diagnostics.

In addition to calculating  $\gamma_{IAV}$  for the CMIP5 ensemble members using simulated atmospheric  $CO_2$ , which most closely resembles the observations available to evaluate ESMs, we calculated  $\gamma_{IAV}$  directly from an area-weighted integral of NBP. This quantity represents the apparent  $CO_2$  growth rate that would be measured in an instantaneously well-mixed atmosphere and contains a source of bias in addition to those described above since it further lacks the imprint of atmospheric mixing. We calculated  $\gamma_{IAV}$  by regressing globally integrated NBP at both monthly and annual time steps against the tropical temperature anomaly, similar to the method used for atmospheric  $CO_2$ . We also calculated  $\gamma_{IAV}$  from NBP confined to the tropics. In terms of developing a tropical functional response metric, this is the most relevant target; however, it is a quantity that is not directly observed. Thus, much of the focus of this paper is on identifying an atmospheric-based metric that can be used to evaluate the  $\gamma_{IAV}$  inferred from model tropical NBP and temperature variations. Since both the NBP and the temperature anomalies were centered in the middle of the calendar month or year, we simply used monthly or annual land temperature averages, rather than averaging two successive time periods, as was required for the regressions against the atmospheric  $CO_2$  growth rate.

### 2.3. Calculating a constraint on $\gamma_{LT}$

We calculated an emergent constraint on the long-term temperature sensitivity of terrestrial carbon storage  $\gamma_{LT}^{opt}$  based on the agreement of  $\gamma_{IAV}$  calculated from annual model data (described in [section 2.2](#)) with the observed  $\gamma_{IAV}^{obs}$  ([section 2.1](#)). We used the  $\gamma_{LT}$  value for each CMIP5 model reported in [Wenzel et al. \(2014\)](#), which were calculated from simulations with a 1% increase in radiative forcing by comparing the response in runs with and without biogeochemical coupling. We fit a slope and intercept to the  $\gamma_{IAV}$  and  $\gamma_{LT}$  data, allowing error in both variables ([York et al. 2004](#)). To parameterize errors on  $\gamma_{IAV}$ , we used the standard deviation from bootstrap Monte Carlo, and we set the errors on  $\gamma_{LT}$  to  $10 \text{ PgC K}^{-1}$ , the value that minimized the reduced  $\chi^2$  value of the fit. It was necessary to assume an error on each model's  $\gamma_{LT}$  to obtain reasonable error estimates on the regression coefficients. The error affected the width of the probability density function for the constrained  $\gamma_{LT}^{opt}$ ; however, the constrained estimate for  $\gamma_{LT}^{opt}$  was insensitive to the choice of the error between 1 and  $30 \text{ PgC K}^{-1}$ . We derived the probability density function for  $\gamma_{LT}^{opt}$  by propagating the uncertainty in the observational constraint ( $\gamma_{IAV}^{obs}$  calculated at the corresponding monthly or annual time step) and the error on the fitted slope and intercept.

## 3. Results

### 3.1. Temperature sensitivities inferred from atmospheric $CO_2$ observations

The observed temperature sensitivity of land carbon uptake ( $\gamma_{IAV}^{obs}$ ) depended strongly on the season analyzed and the frequency over which observations were

averaged (Figure 2). The  $\gamma_{IAV}^{obs}$  determined from annual mean data was  $6.5 \pm 1.1$  PgC yr<sup>-1</sup> K<sup>-1</sup> (Figure 2a), compared to a value of  $5.4 \pm 1.3$  PgC yr<sup>-1</sup> K<sup>-1</sup> determined from monthly data (Figure 2b). Both values for  $\gamma_{IAV}^{obs}$  are consistent with previous estimates from global atmospheric CO<sub>2</sub> (Cox et al. 2013; Keppel-Aleks et al. 2014), but it is worth noting that the methodological uncertainty (a 1.1 PgC yr<sup>-1</sup> K<sup>-1</sup> difference between annual and monthly averaging) is as large as the uncertainty on the fits themselves (1.1–1.3 PgC yr<sup>-1</sup> K<sup>-1</sup>). Calculating  $\gamma_{IAV}$  separately for each quarter revealed strong seasonality to the relationship between the atmospheric CO<sub>2</sub> growth rate and tropical temperature variations (Figures 2c–f). The quarterly growth rate for the NH spring (Figure 2d) had the highest slope ( $5.9 \pm 2.2$ ), while the quarterly growth rate centered on fall (Figure 2f) had a modest temperature sensitivity ( $2.4 \pm 1.0$ ). When quarterly regressions between the CO<sub>2</sub> growth rate and temperature anomalies were performed for NH CO<sub>2</sub> and tropical CO<sub>2</sub> separately, we found weaker correlations (not shown), suggesting that it was necessary to aggregate CO<sub>2</sub> observations from stations globally to define a relevant constraint for model benchmarking.

When the monthly or quarterly CO<sub>2</sub> growth rate and tropical temperature anomalies were recentered by the annual mean values before fitting a  $\gamma_{IAV}$  value, there were only weak relationships between the two quantities (Figure 3), suggesting that global CO<sub>2</sub> growth rate anomalies are most responsive to slowly varying temperature anomalies at annual time scales, as opposed to more rapid fluctuations in temperature at monthly time scales. We note that there is little structure to the residuals as a function of time (colors in Figure 3). The slopes fit to monthly and seasonal residuals were generally weakly positive (Figures 3a–d), with the exception of fall residuals (Figure 3e), indicating that high-frequency temperature stress induced further net carbon release to the atmosphere (Figures 3b–d). For NH fall, the residuals were negatively correlated (Figure 3e), suggesting that after accounting for annual mean temperature anomalies, anomalously warm autumns were associated with more carbon uptake.

### 3.2. A functional response metric for $\gamma_{IAV}$ for tropical ecosystem fluxes

Since our goal was to develop a functional response metric for the tropical ecosystem temperature sensitivity, we first analyzed the difference in temperature sensitivity owing to tropical versus global fluxes. In section 3.1., we showed that annual temperature variations were a more important driver of variations in the observed CO<sub>2</sub> growth rate than temperature variations at higher frequencies; therefore, we analyzed the annually integrated response of land carbon fluxes from CMIP5 simulations. Across the model ensemble, the  $\gamma_{IAV}$  values inferred from both global and tropical NBP spanned an order of magnitude due to differences among model structures and parameterizations (Table 3), consistent with previous results (Wenzel et al. 2014). For most individual models, the temperature sensitivity of tropical land fluxes was different from the temperature sensitivity calculated from global fluxes. Across the model ensemble, the ratio of these two sensitivities ranges from 0.5 to 1.2, with a median value of 0.9. This is a key result because it confirms that for most of the models (six out of eight), extratropical carbon fluxes are also positively correlated with tropical temperature variations, consistent with a prominent role for El Niño–driven teleconnections outside the tropics (Keppel-Aleks et al. 2014). With respect to

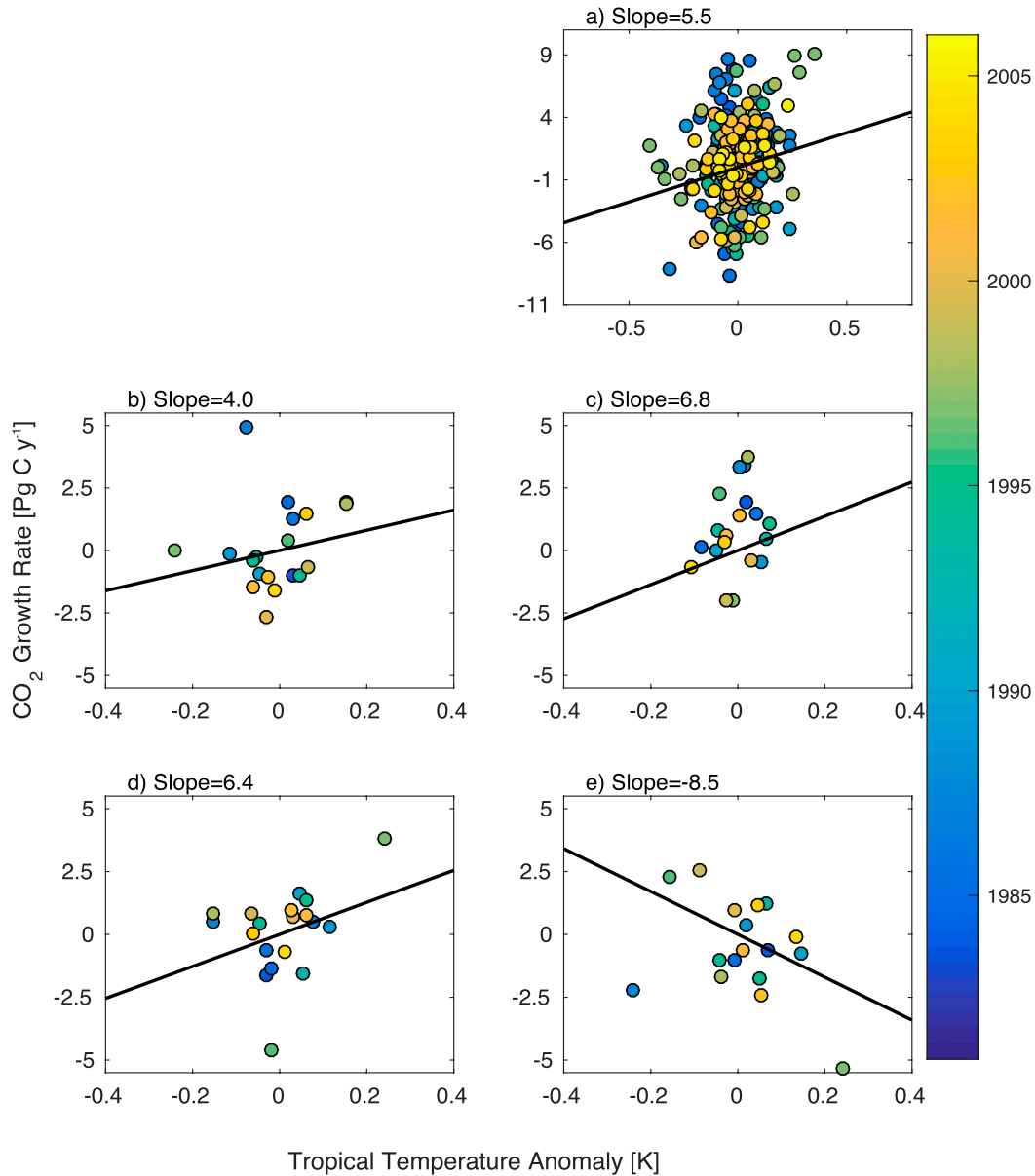


**Figure 3.** Relationship between observed CO<sub>2</sub> growth rate anomaly and tropical temperature variations when each quantity has been recentered by the annual mean. The fit between the residuals is shown at (a) monthly and seasonal time scales for (b) winter (JFM), (c) spring (AMJ), (d) summer (JAS), and (e) fall (OND).

model evaluation, it confirms that the use of global diagnostics (e.g., globally integrated fluxes or the global atmospheric growth rate) to make inferences about the tropics introduces substantial bias.

Second, we analyzed the impact that atmospheric transport leaves on  $\gamma_{IAV}$  by comparing results from globally integrated land fluxes with those from

atmospheric CO<sub>2</sub>. For most models, the  $\gamma_{IAV}$  derived from annual NBP was smaller than that derived from annual CO<sub>2</sub> growth rate, with differences from  $-5\%$  to  $200\%$  (Table 3). On average, the atmospheric CO<sub>2</sub> growth rate within a model was  $30\%$  larger than the corresponding annual integrated net fluxes. If the atmospheric CO<sub>2</sub> time series derived from the available MBL stations were representative of the entire atmosphere, this quantity would be unity by mass balance. The  $30\%$  average difference arises from atmospheric transport processes. Because we used the same atmospheric transport to advect terrestrial fluxes for all members of the ensemble, the different ratio from model to model was due to cross-model differences in the spatial distribution of fluxes relative to dominant patterns of atmospheric transport.

Throughout the manuscript, we calculated the atmospheric CO<sub>2</sub> growth rate from a subset of atmospheric observations within the MBL. Typically, air samples are obtained at these sites within 100 m of the surface; therefore, this type of observation does not reflect the vertical gradients in CO<sub>2</sub> that arise due to the interaction of atmospheric transport and fluxes at the surface. As a sensitivity test, we calculated the total column-integrated CO<sub>2</sub> mole fraction from the GEOS-Chem model output at the same MBL sites, emulating the total column CO<sub>2</sub> currently observed by satellites, such as *OCO-2* (Eldering et al. 2017) and *GOSAT* (Yokota et al. 2009). When using total column CO<sub>2</sub>, the ratio between  $\gamma_{IAV}$  calculated from fluxes and from atmospheric total column CO<sub>2</sub> was reduced but still represented a  $20\%$  mismatch, owing to the fact that the spatially sparse sampling network is not uniformly sensitive to global vegetated land surfaces.

Together, these results suggest that a functional response metric to evaluate the temperature sensitivity of tropical ecosystems should be 1) minimally sensitive to the imprint of extratropical fluxes to better isolate the temperature sensitivity of tropical fluxes and 2) maximally representative of the spatially integrated fluxes despite sparse atmospheric sampling. With these criteria in mind, the relationship between the tropical land-derived  $\gamma_{IAV}$  and the atmosphere-derived  $\gamma_{IAV}$  was highest among CMIP5 models when  $\gamma_{IAV}$  was calculated using the January-centered (winter) atmospheric CO<sub>2</sub> growth rate (Figure 4). Using the seasonal diagnostic, the slope between  $\gamma_{IAV}$  from tropical fluxes and  $\gamma_{IAV}$  from atmospheric CO<sub>2</sub> was  $0.9 \pm 0.3$  ( $R^2 = 0.86$ ), showing both improved correlation and smaller error on the slope, compared to the relationship between the annual growth rate and tropical fluxes (slope of  $1.2 \pm 0.8$  and  $R^2 = 0.71$ ). In other seasons, the  $R^2$  value ranged from 0.4 to 0.7, the slope showed greater deviation from 1, and there was larger fractional uncertainty on the slope.

The strong relationship between tropical land-derived  $\gamma_{IAV}$  and the winter atmospheric-derived  $\gamma_{IAV}$  arises from a seasonally quiescent Northern Hemisphere biosphere. This result was corroborated in two ways: first, the relationship between Northern Hemisphere land-derived  $\gamma_{IAV}$  and the  $\gamma_{IAV}$  derived from the winter CO<sub>2</sub> growth rate was minimal for the winter quarter output ( $R^2 < 0.05$ ), suggesting that Northern Hemisphere ecosystems do not contribute to the seasonal temperature sensitivity. Second, the  $\gamma_{IAV}$  value from winter-only tropical land fluxes was highly correlated with the  $\gamma_{IAV}$  value from winter atmospheric CO<sub>2</sub>, with a slope of  $1.0 \pm 0.2$  and an  $R^2$  of 0.96, confirming minimal interference from the Northern Hemisphere biosphere during the winter season. Together, these relationships confirmed that the winter atmospheric  $\gamma_{IAV}$  value isolates the temperature sensitivity of the tropical carbon–climate functional responses.

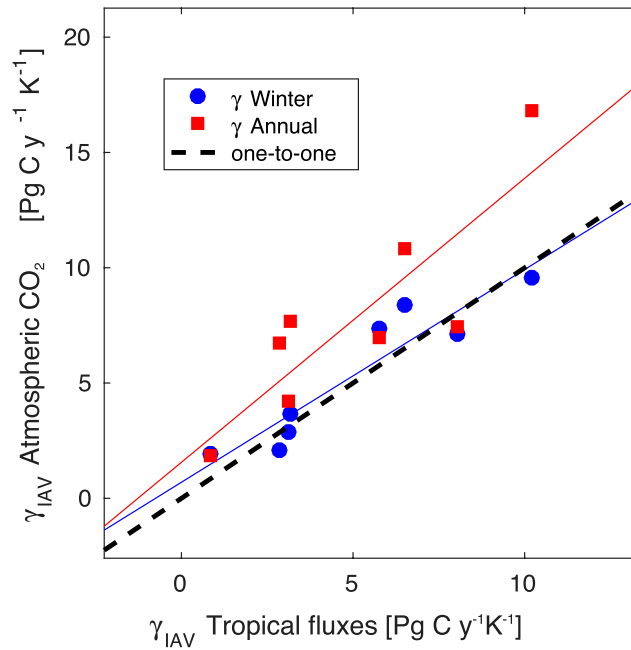


**Figure 4.** Relationship for  $\gamma_{IAV}$  derived from tropical carbon fluxes (x axis) and the corresponding  $\gamma_{IAV}$  calculated from the atmospheric CO<sub>2</sub> growth rate. Parameter  $\gamma_{IAV}$  inferred from winter atmospheric CO<sub>2</sub> observations (red squares) more closely reflects the  $\gamma_{IAV}$  calculated directly from land fluxes across ESMs (slope  $0.9 \pm 0.3$ ,  $R^2 = 0.86$ ), compared to  $\gamma_{IAV}$  from annual CO<sub>2</sub> observations (blue circles; slope  $1.2 \pm 0.8$ ,  $R^2 = 0.71$ ).

### 3.3. An emergent constraint on long-term tropical sensitivity

The winter CO<sub>2</sub> growth rate metric can be used not only to evaluate model representations of tropical carbon fluxes at contemporary time scales, but also to calculate an emergent constraint on the long-term sensitivity of tropical carbon fluxes. When the  $\gamma_{IAV}$  value derived from tropical NBP in each CMIP5 model (Table 3) was evaluated against the observed  $\gamma_{IAV}$  from winter CO<sub>2</sub> growth rate, the estimated long-term climate sensitivity was  $58 \pm 16 \text{ PgC K}^{-1}$  (Figures 5a, 6), in contrast to a value of  $71 \pm 16 \text{ PgC K}^{-1}$  when the observational constraint is from annual CO<sub>2</sub> growth rate (Figures 5b, 6). The 20% high bias when using annual, rather than seasonal, atmospheric CO<sub>2</sub> results from the positive sensitivity between temperature and Northern Hemisphere fluxes for seasons other than NH winter. Extratropical fluxes thereby increased the apparent tropical temperature sensitivity, and a subset of models with greater interannual sensitivity was identified as consistent. In contrast, when the winter  $\gamma_{IAV}$  was used, the consistent model ensemble was weighted toward a lower long-term sensitivity (Figures 5a,b). As expected, the optimized  $\gamma_{LT}$  value was consistent when CMIP5  $\gamma_{IAV}$  values were calculated from each model's winter CO<sub>2</sub> growth rate (Figure 5c), as opposed to directly from tropical land (Figure 5a). We found, however, that both these values were shifted toward a higher sensitivity than the emergent constraint on  $\gamma_{LT}$  derived from annual

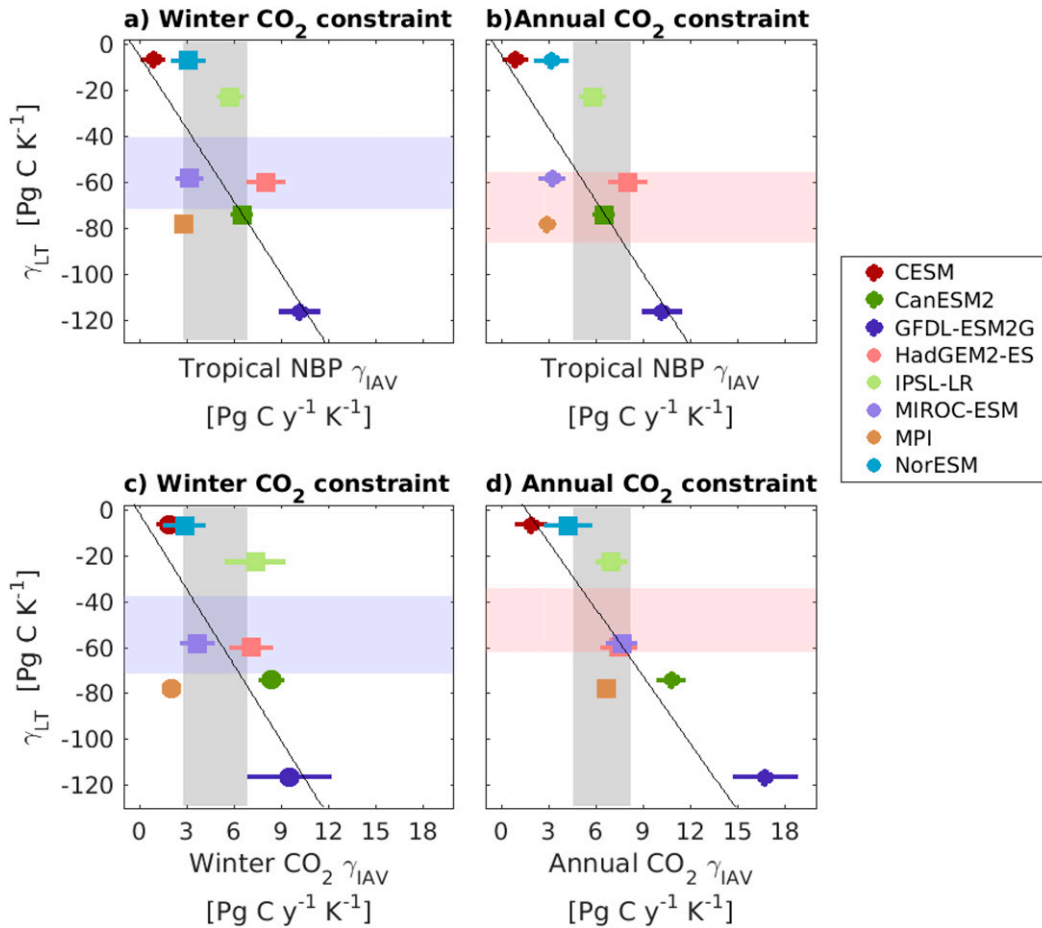


**Figure 5.** Emergent constraint on the long-term sensitivity of tropical ecosystems to climate change ( $\gamma_{LT}$ ). (a),(b) The  $\gamma_{IAV}$  from models is calculated only using tropical NBP fluxes. (c) The model-derived  $\gamma_{IAV}$  is from the winter  $CO_2$  growth rate. (d) The  $\gamma_{IAV}$  values were calculated using the annual  $CO_2$  growth rate. The observational constraint (gray shading) is the winter season  $\gamma_{IAV}$  from atmospheric  $CO_2$  for (a),(c), leading to the constrained  $\gamma_{LT}$  values shown by blue shading. For (b),(d), the emergent constraint is calculated using the annual mean  $\gamma_{IAV}$  from  $CO_2$ , leading to different estimates for  $\gamma_{LT}$  (red shading). For each permutation of model variable and observational constraint, a different set of models is consistent with the observational benchmark (square symbols).

$CO_2$  (Figure 5d;  $48 \pm 14 \text{ PgC K}^{-1}$ ). Again, it is noteworthy that the methodology used to determine the observational constraint introduces as much uncertainty into the emergent constraint ( $13 \text{ PgC K}^{-1}$ ) as does the uncertainty in the fit itself.

#### 4. Discussion

Our results suggest that atmospheric observations can provide direct constraints on tropical land fluxes. We identified a functional response metric to diagnose the

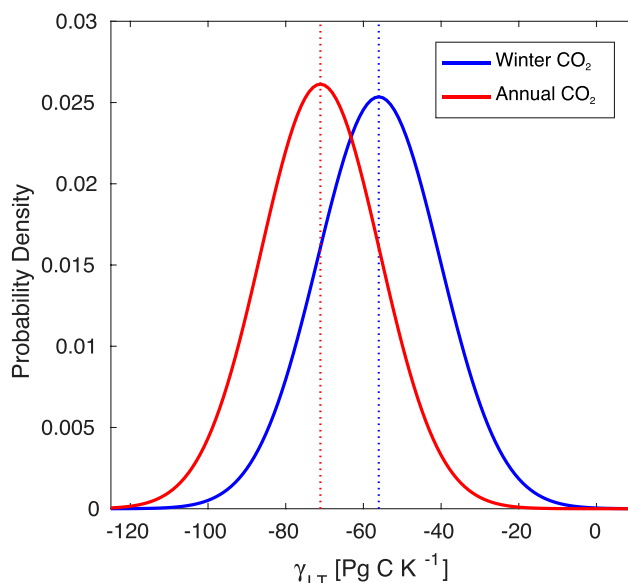


**Figure 6.** Probability density functions for the long-term sensitivity of ecosystem fluxes to climate change ( $\gamma_{LT}$ ). The  $\gamma_{LT}$  for the tropics, constrained by winter  $\text{CO}_2$  data, is  $58 \pm 16 \text{ PgC K}^{-1}$ , 20% less sensitive than when the emergent constraint is defined by annual  $\text{CO}_2$  data ( $71 \pm 16 \text{ PgC K}^{-1}$ ). The shift in the most likely value for  $\gamma_{LT}$  due to the methodology used to average observations is as large as the uncertainty on the fit itself.

sensitivity of tropical carbon fluxes to local temperature variations using the winter seasonal atmospheric  $\text{CO}_2$  growth rate. When winter atmospheric  $\text{CO}_2$  growth rate anomalies were used to evaluate the temperature sensitivity of net tropical ecosystem exchange, the interference from Northern Hemisphere ecosystems was minimized. Additionally, bias from sparse atmospheric  $\text{CO}_2$  sampling was small, based on offline analysis from eight CMIP5 ESMs whose terrestrial fluxes have been advected using an atmospheric tracer transport model. We found that a different set of models was consistent with the observational constraint, depending on whether atmospheric  $\text{CO}_2$  data were integrated annually versus isolating only one season, a finding that affects the benchmarking and subsequent tuning of ESMs. In this study, six ESMs whose tropical  $\gamma_{IAV}$  ranged from  $2.8$  to  $8.1 \text{ PgC yr}^{-1} \text{ K}^{-1}$  were consistent with the observational constraint. Moreover, we found that the predicted long-term temperature sensitivity of tropical ecosystems was  $58 \pm 16 \text{ PgC K}^{-1}$ , a value that was smaller by 20% than if an annual constraint had been used.

Atmospheric  $\text{CO}_2$  observations provide one of the few regional- to global-scale diagnostics for carbon cycle processes. Although atmospheric  $\text{CO}_2$  has been used previously for model benchmarking in terms of the long-term increase (Hoffman et al. 2014) or seasonal diagnostic (Keppel-Aleks et al. 2013), determining functional responses that can be used to benchmark large-scale feedbacks in the context of biogeochemical and land model benchmarking systems [e.g., the International Land Model Benchmarking Project (ILAMB); Mu et al. 2014; Hoffman et al. 2017]

is important for improving the predictions of terrestrial models. Determining robust ways to work with atmospheric CO<sub>2</sub> presents challenges, however, since it integrates land, ocean, and anthropogenic fluxes over a range of geographic scales. Developing a CO<sub>2</sub> metric that isolates a single functional response, as we have done here, opens up possibilities to use observations in different ways to isolate each of these different sensitivities that control long-term feedbacks. Especially in the context of an emergent constraint, tropical and Northern Hemisphere ecosystems will likely experience different responses to long-term temperature increases and, thus, must be considered separately.

In the context of an emergent constraint, our analysis shows that different averaging time scales for the observations affect the optimized constraint, as does using atmospheric CO<sub>2</sub> to evaluate land fluxes directly, rather than evaluating fluxes transported through an atmospheric model. In the introduction, we identified two key components to an emergent constraint: the ability to evaluate short-term predictions against observations and a mechanistic link between the short- and long-term model-predicted quantities. While substantial attention has been paid in the literature to concerns that long-term feedbacks may include processes that do not contribute substantially to present-day interannual variability in land carbon storage (Randerson 2013; Keppel-Aleks et al. 2014), less attention has been given to how differences among model output and observations affect an emergent constraint. Here, we showed that there is potential for bias in emergent constraints when the differences between observed and simulated quantities are ignored. In fact, our results suggest that the method used to average the observational constraint for functional response metrics or for emergent constraints is as important as the fitting uncertainty itself.

Our results indicated that the emergent constraint on terrestrial temperature sensitivity from a multimodel ensemble shows a systematic dependence on the choice of observational constraint and the treatment of model output. There was a 20% difference in the expected value for the tropical  $\gamma_{LT}$  when the annual versus winter atmospheric CO<sub>2</sub> growth rate was used to evaluate short-term variations. This difference can be explained by the fact that annual CO<sub>2</sub> growth rate anomalies include the additional temperature sensitivity of extratropical Northern Hemisphere ecosystems. It is more difficult to explain, however, why the emergent constraint on  $\gamma_{LT}$  derived from the annual CO<sub>2</sub> growth rate from CMIP5 models and as the observational constraint (Fig. 5d) yields a lower value for  $\gamma_{LT}$  ( $48 \pm 14$  PgC K<sup>-1</sup>), beyond noting that small differences in the  $\gamma_{IAV}$  values can lead to large differences in the fitted slope. Thus, the error on the optimized  $\gamma_{LT}$  may be underestimated by the error propagation and quantification methods generally used in the calculation of emergent constraints. The error on  $\gamma_{LT}$  may further be underestimated because the interannual variations in the CO<sub>2</sub> growth rate used to calculate  $\gamma_{LT}$  may not be predictive of nonlinearities within the carbon cycle due to, for example, changes in vegetation mortality or fire, which are not well represented in CMIP5 ESMs. These nonlinearities may change the long-term trajectory of tropical ecosystems and invalidate the entire approach of calculating an emergent constraint.

Given the persistent uncertainties in prediction of the land carbon sink over the twenty-first century and the fact that CMIP5 coupled models simulated as large of a spread in cumulative net carbon uptake as did an earlier generation of C<sup>4</sup>MIP models (Friedlingstein et al. 2006, 2014), analyzing model output fields that have

direct relationships to observational datasets is crucial. Our results show that there is a 25% bias when  $\gamma_{\text{IAV}}$  was calculated from atmospheric data versus integrated NBP within the model ensemble (Table 2). In the analysis presented here, it was necessary to translate fluxes through a transport model or emulator to reproduce model data as similar to the atmospheric observations as possible. However, using atmospheric transport inconsistent with the climate used to force land surface fluxes contributes additional uncertainty that could be avoided by making the time-varying, three-dimensional structure of atmospheric CO<sub>2</sub> a standard model output.

**Acknowledgments.** The research was supported in part by the RUBISCO Scientific Focus Area (SFA), which is sponsored by the Regional and Global Climate Modeling (RGCM) Program in the Climate and Environmental Sciences Division (CESD) of the Office of Biological and Environmental Research in the U.S. Department of Energy Office of Science. Oak Ridge National Laboratory is managed by UT-Battelle, LLC, for the U.S. Department of Energy under Contract DE-AC05-00OR22725. We acknowledge the World Climate Research Programme’s Working Group on Coupled Modelling, which is responsible for CMIP, and we thank the climate modeling groups producing and making available their model output. For CMIP, the U.S. Department of Energy’s Program for Climate Model Diagnosis and Intercomparison provides coordinating support and led development of software infrastructure in partnership with the Global Organization for Earth System Science Portals.

## References

- Ahlström, A., and Coauthors, 2015: The dominant role of semi-arid ecosystems in the trend and variability of the land CO<sub>2</sub> sink. *Science*, **348**, 895–899, <https://doi.org/10.1126/science.aaa1668>.
- Araujo, A. C., and Coauthors, 2002: Comparative measurements of carbon dioxide fluxes from two nearby towers in a central Amazonian rainforest: The Manaus LBA site. *J. Geophys. Res.*, **107**, 8090, <https://doi.org/10.1029/2001JD000676>.
- Arora, V. K., and Coauthors, 2013: Carbon–concentration and carbon–climate feedbacks in CMIP5 Earth system models. *J. Climate*, **26**, 5289–5314, <https://doi.org/10.1175/JCLI-D-12-00494.1>.
- Battle, M., M. L. Bender, P. P. Tans, J. W. C. White, J. T. Ellis, T. Conway, and R. J. Francey, 2000: Global carbon sinks and their variability inferred from atmospheric O<sub>2</sub> and  $\delta^{13}\text{C}$ . *Science*, **287**, 2467–2470, <https://doi.org/10.1126/science.287.5462.2467>.
- Bear, C., and Coauthors, 2010: Terrestrial gross carbon dioxide uptake: Global distribution and covariation with climate. *Science*, **329**, 834–838, <https://doi.org/10.1126/science.1184984>.
- Boé, J., A. Hall, and X. Qu, 2009: September sea-ice cover in the Arctic Ocean projected to vanish by 2100. *Nat. Geosci.*, **2**, 341–343, <https://doi.org/10.1038/ngeo467>.
- Boer, G. J., and V. Arora, 2009: Temperature and concentration feedbacks in the carbon cycle. *Geophys. Res. Lett.*, **36**, L02704, <https://doi.org/10.1029/2008GL036220>.
- Bonan, G. B., and S. C. Doney, 2018: Climate, ecosystems, and planetary futures: The challenge to predict life in Earth system models. *Science*, **359**, eaam8328, <https://doi.org/10.1126/science.aam8328>.
- Chapin, F. S., and Coauthors, 2006: Reconciling carbon-cycle concepts, terminology, and methods. *Ecosystems*, **9**, 1041–1050, <https://doi.org/10.1007/s10021-005-0105-7>.
- Conway, T. J., P. P. Tans, L. S. Waterman, K. W. Thoning, D. R. Kitzis, K. A. Masarie, and N. Zhang, 1994: Evidence for interannual variability of the carbon cycle from the National Oceanic and Atmospheric Administration/Climate Monitoring and Diagnostics Laboratory

- global air sampling network. *J. Geophys. Res.*, **99**, 22 831–22 855, <https://doi.org/10.1029/94JD01951>.
- Cox, P. M., D. Pearson, B. B. Booth, P. Friedlingstein, C. Huntingford, C. D. Jones, and C. M. Luke, 2013: Sensitivity of tropical carbon to climate change constrained by carbon dioxide variability. *Nature*, **494**, 341–344, <https://doi.org/10.1038/nature11882>.
- Dlugokencky, E. J., P. M. Lang, J. W. Mund, A. M. Crotwell, M. J. Crotwell, and K. W. Thoning, 2016: Atmospheric carbon dioxide dry air mole fractions from the NOAA ESRL carbon cycle cooperative global air sampling network, 1968–2015, version 2016-08-30. NOAA, accessed 4 January 2017, [ftp://aftp.cmdl.noaa.gov/data/trace\\_gases/co2/flask/surface/](ftp://aftp.cmdl.noaa.gov/data/trace_gases/co2/flask/surface/).
- Doughty, C. E., and M. L. Goulden, 2008: Are tropical forests near a high temperature threshold? *J. Geophys. Res.*, **113**, G00B07, <https://doi.org/10.1029/2007JG000632>.
- Eldering, A., and Coauthors, 2017: The Orbiting Carbon Observatory-2: First 18 months of science data products. *Atmos. Meas. Tech.*, **10**, 549–563, <https://doi.org/10.5194/amt-10-549-2017>.
- Friedlingstein, P., and Coauthors, 2006: Climate–carbon cycle feedback analysis: Results from the C<sup>4</sup>MIP Model Intercomparison. *J. Climate*, **19**, 3337–3353, <https://doi.org/10.1175/JCLI3800.1>.
- , M. Meinshausen, V. K. Arora, C. D. Jones, A. Anav, S. K. Liddicoat, and R. Knutti, 2014: Uncertainties in CMIP5 climate projections due to carbon cycle feedbacks. *J. Climate*, **27**, 511–526, <https://doi.org/10.1175/JCLI-D-12-00579.1>.
- Gatti, L. V., and Coauthors, 2014: Drought sensitivity of Amazonian carbon balance revealed by atmospheric measurements. *Nature*, **506**, 76–80, <https://doi.org/10.1038/nature12957>.
- Gordon, N. D., and S. A. Klein, 2014: Low-cloud optical depth feedback in climate models. *J. Geophys. Res. Atmos.*, **119**, 6052–6065, <https://doi.org/10.1002/2013JD021052>.
- Hall, A., and X. Qu, 2006: Using the current seasonal cycle to constrain snow albedo feedback in future climate change. *Geophys. Res. Lett.*, **33**, L03502, <https://doi.org/10.1029/2005GL025127>.
- Hoffman, F. M., and Coauthors, 2014: Causes and implications of persistent atmospheric carbon dioxide biases in Earth system models. *J. Geophys. Res. Biogeosci.*, **119**, 141–162, <https://doi.org/10.1002/2013JG002381>.
- , and Coauthors, 2017: International Land Model Benchmarking (ILAMB) 2016 workshop report. U.S. DOE Tech. Rep. DOE/SC-0186, 172 pp., <https://doi.org/10.2172/1330803>.
- Jones, P. D., D. H. Lister, T. J. Osborn, C. Harpham, M. Salmon, and C. P. Morice, 2012: Hemispheric and large-scale land-surface air temperature variations: An extensive revision and an update to 2010. *J. Geophys. Res.*, **117**, D05127, <https://doi.org/10.1029/2011JD017139>.
- Keppel-Aleks, G., and Coauthors, 2013: Atmospheric carbon dioxide variability in the Community Earth System Model: Evaluation and transient dynamics during the twentieth and twenty-first centuries. *J. Climate*, **26**, 4447–4475, <https://doi.org/10.1175/JCLI-D-12-00589.1>.
- , and Coauthors, 2014: Separating the influence of temperature, drought, and fire on interannual variability in atmospheric CO<sub>2</sub>. *Global Biogeochem. Cycles*, **28**, 1295–1310, <https://doi.org/10.1002/2014GB004890>.
- Klein, S. A., and A. Hall, 2015: Emergent constraints for cloud feedbacks. *Curr. Climate Change Rep.*, **1**, 276–287, <https://doi.org/10.1007/s40641-015-0027-1>.
- Le Quéré, C., and Coauthors, 2016: Global carbon budget 2016. *Earth Syst. Sci. Data*, **8**, 605–649, <https://doi.org/10.5194/essd-8-605-2016>.
- Mu, M., F. M. Hoffman, D. M. Lawrence, W. J. Riley, G. Keppel-Aleks, E. B. Kluzek, C. D. Koven, and J. T. Randerson, 2014: Model evaluation using a community benchmarking system for land surface models. *2014 Fall Meeting*, San Francisco, CA, Amer. Geophys. Union, Abstract B23C-0209.
- Nassar, R., and Coauthors, 2010: Modeling global atmospheric CO<sub>2</sub> with improved emission inventories and CO<sub>2</sub> production from the oxidation of other carbon species. *Geosci. Model Dev.*, **3**, 689–716, <https://doi.org/10.5194/gmd-3-689-2010>.
- Pan, Y., and Coauthors, 2011: A large and persistent carbon sink in the world’s forests. *Science*, **333**, 988–993, <https://doi.org/10.1126/science.1201609>.

- Phillips, O. L., and Coauthors, 2009: Drought sensitivity of the Amazon rainforest. *Science*, **323**, 1344–1347, <https://doi.org/10.1126/science.1164033>.
- Randerson, J. T., 2013: Climate science: Global warming and tropical carbon. *Nature*, **494**, 319–320, <https://doi.org/10.1038/nature11949>.
- , and Coauthors, 2009: Systematic assessment of terrestrial biogeochemistry in coupled climate–carbon models. *Global Change Biol.*, **15**, 2462–2484, <https://doi.org/10.1111/j.1365-2486.2009.01912.x>.
- Rayner, P. J., R. M. Law, C. E. Allison, R. J. Francey, C. M. Trudinger, and C. Pickett-Heaps, 2008: Interannual variability of the global carbon cycle (1992–2005) inferred by inversion of atmospheric CO<sub>2</sub> and δ<sup>13</sup>CO<sub>2</sub> measurements. *Global Biogeochem. Cycles*, **22**, GB3008, <https://doi.org/10.1029/2007GB003068>.
- Rienecker, M. M., and Coauthors, 2011: MERRA: NASA’s Modern-Era Retrospective Analysis for Research and Applications. *J. Climate*, **24**, 3624–3648, <https://doi.org/10.1175/JCLI-D-11-00015.1>.
- Schimel, D., and Coauthors, 2015: Observing terrestrial ecosystems and the carbon cycle from space. *Global Change Biol.*, **21**, 1762–1776, <https://doi.org/10.1111/gcb.12822>.
- Taylor, K. E., R. J. Stouffer, and G. A. Meehl, 2012: An overview of CMIP5 and the experiment design. *Bull. Amer. Meteor. Soc.*, **93**, 485–498, <https://doi.org/10.1175/BAMS-D-11-00094.1>.
- Tebaldi, C., and R. Knutti, 2007: The use of the multi-model ensemble in probabilistic climate projections. *Philos. Trans. Roy. Soc. London*, **365A**, 2053–2075, <https://doi.org/10.1098/rsta.2007.2076>.
- Townsend, A. R., G. P. Asner, and C. C. Cleveland, 2008: The biogeochemical heterogeneity of tropical forests. *Trends Ecol. Evol.*, **23**, 424–431, <https://doi.org/10.1016/j.tree.2008.04.009>.
- Wang, W., and Coauthors, 2013: Variations in atmospheric CO<sub>2</sub> growth rates coupled with tropical temperature. *Proc. Nat. Acad. Sci.*, **110**, 13 061–13 066, <https://doi.org/10.1073/pnas.1219683110>.
- Wenzel, S., P. M. Cox, V. Eyring, and P. Friedlingstein, 2014: Emergent constraints on climate–carbon cycle feedbacks in the CMIP5 Earth system models. *J. Geophys. Res. Biogeosci.*, **119**, 794–807, <https://doi.org/10.1002/2013JG002591>.
- Williams, D. N., and Coauthors, 2011: The Earth System Grid Federation: Software framework supporting CMIP5 data analysis and dissemination. *CLIVAR Exchanges*, No. 56, International CLIVAR Project Office, Southampton, United Kingdom, 40–42.
- Wunch, D., and Coauthors, 2013: The covariation of Northern Hemisphere summertime CO<sub>2</sub> with surface temperature in boreal regions. *Atmos. Chem. Phys.*, **13**, 9447–9459, <https://doi.org/10.5194/acp-13-9447-2013>.
- Yokota, T., Y. Yoshida, N. Eguchi, Y. Ota, T. Tanaka, H. Watanabe, and S. Maksyutov, 2009: Global concentrations of CO<sub>2</sub> and CH<sub>4</sub> retrieved from GOSAT: First preliminary results. *SOLA*, **5**, 160–163, <https://doi.org/10.2151/sola.2009-041>.
- York, D., N. M. Evensen, M. L. Martínez, and J. D. Delgado, 2004: Unified equations for the slope, intercept, and standard errors of the best straight line. *Amer. J. Phys.*, **72**, 367, <https://doi.org/10.1119/1.1632486>.